Torsional deformations in incompressible fibre–reinforced cylindrical pipes

P. Nardinocchi, T. Svatoň, L. Teresi

Accepted Manuscript

Title: Torsional deformations in incompressible fibre–reinforced cylindrical pipes

Authors: P. Nardinocchi, T. Svatoň, L. Teresi

PII: S0997-7538(09)00112-0

DOI: 10.1016/j.euromechsol.2009.09.001

Reference: EJMSOL 2547

To appear in: *European Journal of Mechanics / A Solids*

Received Date: 7 May 2009

Revised Date: 13August2009

Accepted Date: 13 September 2009

Please cite this article as: Nardinocchi, P. Svatoň, T, Teresi, L.,. Torsional deformations in incompressible fibre–reinforced cylindrical pipes, European Journal of Mechanics / A Solids (2009), doi: 10.1016/j.euromechsol.2009.09.001

Torsional deformations in incompressible fibre–reinforced cylindrical pipes

P. Nardinocchi[*,a], T. Svatoň[b], L. Teresi[c]

[a] *Dipartimento di Ingegneria Strutturale e Geotecnica, Università di Roma "La Sapienza" via Eudossiana 18, I-00147 Roma, Italy,*
[b] *University of West Bohemia, Pilsen, Czech Republic*
[c] *Dipartimento di Strutture, Università Roma Tre, Roma, Italy*

Abstract

The first part of the paper deals with an extension of the classical Rivlin's solution of the torsion problem of a neo-Hookean pipe. The second part concerns a study of the passive torsional deformation processes in a fibre–reinforced cylindrical dummy of the beating heart. Especially, the dependence of the torsional and volumetric stiffness of the cylindrical pipe on different geometric and material parameters is discussed through a set of numerical simulations.

Key words: fibre–reinforced non-linearly incompressible elastic solids, finite torsion
PACS: 46.05.+b, 46.70.Lk

1. Introduction

In the last few years, fibre–reinforced materials have made a new comeback in a new and more appealing biomechanical flavour. In fact, quite a few living materials are characterized by mechanical responses which are strongly anisotropic due to their fibred structure. Accordingly, much attention has been devoted to the modelling issues raised by fibre-reinforced solids undergoing finite deformations (Merodio and Ogden, 2005; Holzapfel et al., 2005, 2004; Gasser et al., 2006). Specifically, we are involved in an extensive work on the electromechanical modeling of left ventricle and a key step of our work concerns the modeling of the passive and active response of cardiac tissue. Typically, myocardium is modeled as an incompressible elastic material reinforced by cardiac muscle fibres which can contract in response to electrophysiological stimuli. As is evident, the overall response of the left ventricle depends on the modeling of both the passive and the active behavior of the cardiac tissue. Here, we deal with the passive behaviour of a fibre–reinforced cylindrical dummy of the left ventricle under torsional deformations and arrange the paper in two, basically disjoint even if related, parts.

The first part concerns homogeneous torsional deformations of helically wound fibre-reinforced incompressible elastic pipes and the analysis of the corresponding non linear boundary value problem is developed explicitly. It is related to the study developed in (Nardinocchi et al., 2009) where the mechanical response of the pipe has been described through the standard quadratic reinforcement model (Merodio and Ogden, 2005). Here, we account for an alternative reinforcement model, always proposed and discussed for special homogeneous deformations in (Merodio and Ogden, 2005), more sensitive to shear deformations and discuss the effects of the two different, even if similar, material models on the homogeneous solution of the torsion problem.

The second part is meant as a first step towards the analysis of the torsional deformation underwent by the left ventricle during the cardiac cycle; the motivation being provided by the fact that left ventricular torsion has been recently recognized as an important indicator of cardiac function (Taber et al., 1996; Nagel et al., 2000). Nevertheless, from a mechanical point of view, little attention has been devoted to the pattern of twist during the cardiac cycle. Specifically, we account for the inhomogeneous torsional deformations induced by a pressure field on the cylinder; still, we do not

[*] Corresponding author
Email addresses: paola.nardinocchi@uniroma1.it (P. Nardinocchi), tsvaton@gmail.com (T. Svatoň), teresi@uniroma3.it (L. Teresi)

care of the active behaviour of the muscle fibres (see (DiCarlo et al., 2009)) for the active behavior modeling) and use the model to study the effects of various material and geometric parameters on the torsional behaviour of the pipe with frozen fibres.

We see that the anisotropy due to the variation in muscle fibre angle across the wall of the pipe induces rotation of one end with respect to the other; nevertheless, rotation is induced in absence of such variation, too, when the fibre angles are fixed across the walls and far from some extreme values. Moreover, the material parameters related to the choice of the reinforcing model afflict the mechanical response of the pipe, too. We show that there is a considerable change in volume related to the pressure field which is influenced by the same material parameters, too. Of course, the pure elasticity of the material does not allow to see any pressure–torsion and pressure–volume loops whose formation is basically related to the active nature of the fibres which change when contracted the ground state of the pipe (see (DiCarlo et al., 2009)). To mimic the cardiac situation, the sensitivity of the torsion of the cylindrical pipe to changes in pipe geometry is studied by simulating two types of excessive development of the cylindrical geometry with respect to the basic one. The first is characterized by an augmented wall thickness (resembling the ventricular eccentric hypertrophy); the second by an augmented lumen (resembling the ventricular concentric hyperthrophy).

2. Fibre-reinforced bodies

Let $\{\mathbf{e}_1, \mathbf{e}_2, \mathbf{e}_3\}$ be an orthonormal basis of the translation space $\mathcal{V}$ of the three–dimensional Euclidean space $\mathcal{E}$ and $\mathcal{U}$ be the orthogonal complement to $\mathtt{span}\{\mathbf{e}_3\}$ with respect to $\mathcal{V}$. Fixed an interval $\mathcal{I} = [0, h] \subset \mathcal{R}$ and a pole $o \in \mathcal{E}$, we consider the axisymmetric pipe-like region $\mathcal{C}$ defined as follows:

$$\mathcal{C} = \{p \in \mathcal{E} : p = o + r\,\mathbf{n}(\theta) + \zeta\,\mathbf{e}_3\}\,, \quad \mathbf{n}(\theta) = \cos\theta\,\mathbf{e}_1 + \sin\theta\,\mathbf{e}_2\,,\ 0 < \theta < 2\pi\,,\ \zeta \in \mathcal{I}\,,\ R_i < r < R_o\,. \tag{2.1}$$

The boundary $\partial\mathcal{C}$ is defined as

$$\partial\mathcal{C} = \mathcal{D}_0 \cup \mathcal{D}_h \cup \mathcal{M}_i \cup \mathcal{M}_o\,, \tag{2.2}$$

with $\mathcal{D}_0$ and $\mathcal{D}_h$ the bases of the pipe and $\mathcal{M}_i$ and $\mathcal{M}_o$ the inner and outer mantle, respectively.

A helix-like fibre of pitch b is a curve whose unit tangent vector $\mathbf{e}_b = \hat{\mathbf{e}}_b(r, \theta)$ at any $p \in \mathcal{C}$ is defined as

$$\hat{\mathbf{e}}_b(r, \theta) = \frac{r}{(r^2 + b^2)^{\frac{1}{2}}}\,\mathbf{n}_{,\theta}\,(\theta) + \frac{b}{(r^2 + b^2)^{\frac{1}{2}}}\,\mathbf{e}_3\,, \tag{2.3}$$

with the subscript b remembering the dependence of the unit tangent vector on the pitch b of the helix. So, at any place $\mathbf{p}$ of a helically wound fibre–reinforced body $\mathcal{C}$, the material fibre $(p, \mathbf{e}_b)$ with $\mathbf{e}_b$ as in (2.3) identifies a locus of material reinforcement; for $b = 0$ equation (2.3) defines a circumferential uniaxial reinforcement ($\mathbf{e}_0(r, \theta) = \mathbf{n}_{,\theta}\,(\theta)$). Sometimes, a different parametrization of the helical curve is referred to, with the pitch b of the helix expressed in terms of the angle α defined as

$$\cos\alpha = \mathbf{e}_b \cdot \mathbf{e}_0\,. \tag{2.4}$$

With (2.3), it turns out

$$\tan\alpha = \frac{b}{r}\,. \tag{2.5}$$

Specifically, the fibre angle α is a relevant parameter for the ventricular geometry where fibres account for anisotropic reinforcement due to collagene, or may represent muscles fibres. In that case, it is important to account for the large variation of the fibres angles across the wall of the left ventricle. Typically, the angle α ranges between $-60°$ (on the outer wall) and $60°$ (on the inner wall) and the anisotropy due to the variation amplifies the ventricular torsion occurring during the cardiac cycle. In (Nardinocchi et al., 2009), we described the material response of the incompressible ($J = 1$) body through the following strain energy function based on the quadratic reinforcement model I_4

$$\psi(\mathbf{C}) = c_1\left(I_1(\mathbf{C}) - 3 + \gamma\,(I_4(\mathbf{C}) - 1)^2\right), \quad I_1(\mathbf{C}) = \mathbf{C} \cdot \mathbf{I}\,, \quad I_4(\mathbf{C}) = \mathbf{C}\mathbf{e}_b \cdot \mathbf{e}_b\,, \quad \mathbf{C} = \mathbf{F}^T\mathbf{F}\,, \tag{2.6}$$

with $\gamma > 0$. In this paper, we consider the strain energy

$$\psi(\mathbf{C}) = c_1\left(I_1(\mathbf{C}) - 3) + \gamma\,(I_5(\mathbf{C}) - 1)^2\right), \quad I_5(\mathbf{C}) = \mathbf{C}^2\mathbf{e}_b \cdot \mathbf{e}_b\,, \tag{2.7}$$

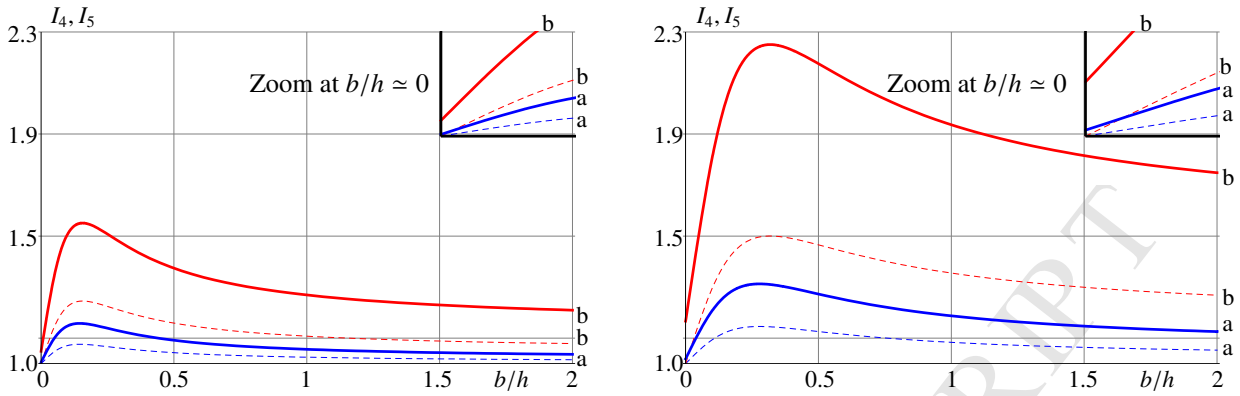

Figure 1: I_4 (dashed lines) and I_5 (solid lines) VS b/h for two different given torsions: $\varphi_h = \pi/6$ (a, blue), $\varphi_h = \pi/2$ (b, red); values on the inner mantle (left), and at the outer mantle (right). Insets at top–right represent a zoom at $b/h \simeq 0$

which, as it is well known (Merodio and Ogden, 2005), is more suited to the present context characterized by large shear deformations. As example, under torsional deformation (Nardinocchi et al., 2009) the quadratic reinforcement tends to become ineffective as the ratio b/h goes to 0, while the reinforcement I_5 is effectual even with circumferential fibres.

3. Pure and homogeneous torsional deformations

As first, we analyze the mechanical response of the helically wound fibre–reinforced incompressible pipe to torsional deformations induced through a torsional rotation of one end of the pipe. An extension of the solution of the pure torsional problem studied for isotropic and incompressible cylinders by Rivlin (Rivlin, 1949) to the material pipe described by the strain energy (2.7) is performed. The same extension has been performed in (Nardinocchi et al., 2009) in presence of the standard quadratic reinforcement model and a comparison of the solutions clarifies the roles of the different reinforcement models in presence of torsional deformations.

A concise representation formula of a pure torsional deformation $\mathbf{f} : C \to \mathcal{E}$ is the following

$$\mathbf{f}(p) = (\mathbf{I} + \sin\varphi\, \mathbf{e}_2 \wedge \mathbf{e}_1 - (1 - \cos\varphi)\, \check{\mathbf{I}})\,(p - o)\,, \quad \varphi = \zeta\,\tau\,, \tag{3.8}$$

where $\mathbf{e}_2 \wedge \mathbf{e}_1 = \mathbf{e}_2 \otimes \mathbf{e}_1 - \mathbf{e}_1 \otimes \mathbf{e}_2$, φ is the *torsion angle*, and τ is the unit torsion angle. From now on, we parametrize the torsional deformation (3.8) through the torsion angle $\hat{\varphi} = h\,\tau$ of $\mathcal{D}_h$. The geometrical structure of the cylinder–like body C is retained under the deformation (3.8) and, denoted with $\mathbf{x} \in \mathcal{V}$ the position vector of the place $x = \mathbf{f}(p)$ with respect to o, it holds:

$$\mathbf{x} = \mathbf{x}_o + \zeta\,\mathbf{e}_3\,, \quad \mathbf{x}_o = r(\cos\varphi\,\mathbf{n}(\theta) + \sin\varphi\,\mathbf{n}_{,\theta}\,(\theta))\,. \tag{3.9}$$

The deformation gradient $\mathbf{F}$ corresponding to (3.8) may be represented as

$$\mathbf{F} = \check{\mathbf{F}} + \tau\,\mathbf{x}_o^* \otimes \mathbf{e}_3 + \mathbf{e}_3 \otimes \mathbf{e}_3\,, \tag{3.10}$$

with $\check{\mathbf{F}} \in \mathbb{L}\mathtt{in}(\mathcal{U})$ and $\mathbf{x}_o^* \in \mathcal{U}$ given by

$$\check{\mathbf{F}} = \cos\varphi\,\check{\mathbf{I}} + \sin\varphi\,(\mathbf{e}_2 \wedge \mathbf{e}_1)\,, \quad \mathbf{x}_o^* = \mathbf{e}_3 \times \mathbf{x}_o\,. \tag{3.11}$$

Let us note that deformation (3.8) identically satisfies the incompressibility constraint $J = \mathtt{det}\mathbf{F} = 1$. The three invariants we are interested in, I_1, I_4, I_5, write as follows

$$I_1 = 3 + r^2\tau^2\,, \quad I_4 = 1 + r\,k(r)\,(2 + b\,\tau)\,b\,\tau\,, \quad I_5 = I_4 + r\,k(r)\,(1 + b\,\tau)\,(2b\,\tau + r^2\tau^2 + r^2\,b\,\tau^3)\,, \tag{3.12}$$

where $k(r) = r\,(r^2 + b^2)^{-1}$ is the curvature of the helix. The invariant I_4 measures the stretch along the material fibre $(p, \mathbf{e}_b)$; it is interesting to note that the stretch I_4 is not a monotone function of the dimensionless pitch b/h and depends weakly on the place $p \in C$.

Figure 1 shows that the behaviour of I_4 versus b/h is qualitatively the same at the inner and at the outer radius. Moreover, it shows that for circumferential fibres ($b/h = 0$) $I_4 \equiv 1$, that is, the fibre length does not change under the torsional deformation (3.8). On the contrary, the invariant I_5 is sensitive to shear deformation too, as it is discussed in (Merodio and Ogden, 2005) for different values of the strength γ of the reinforcement; thus, it happens that I_5 is different from 1 at $b/h = 0$, see zoom in Fig 1. At the end, it is worth noting that at any r between R_i and R_o, there is a value of the dimensionless pitch b/h which gives the maximum fibre stretch; moreover, the same b/h gives the maximum value of I_5, too. When the strain energy function (2.7) is used, the corresponding Cauchy stress is

$$\mathbf{T} = 2c_1\mathbf{B} + 2c_1\gamma\,(I_5 - 1)\,(\mathbf{FCe}_b \otimes \mathbf{Fe}_b + \mathbf{Fe}_b \otimes \mathbf{FCe}_b) - p\,\mathbf{I}\,, \tag{3.13}$$

with $\mathbf{B} = \mathbf{F}\mathbf{F}^T$; the Cauchy stress corresponding to an incompressible neo-Hookean material turns out by setting $\gamma = 0$. The balance equation of the body ($\mathtt{div}\,\mathbf{T} = 0$) gives an explicit representation for p

$$\begin{aligned} p = \hat{p}(r, b, \tau) = {} & p_o(b, \tau) - c_1\,(1 - 2\gamma\,p_1(b, \tau))\,\tau^2\,r^2 - c_1\,\gamma\,(1 + b\,\tau)^4\tau^4\,r^4 \\ & - 2\,c_1\,\gamma\,p_2(b, \tau)\,\log(b^2 + r^2) - 2\,c_1\,\gamma\,p_3(b, \tau)\,\frac{1}{b^2 + r^2}\,, \end{aligned} \tag{3.14}$$

where the function p_o is determined by the boundary conditions, and

$$\begin{aligned} p_1(b, \tau) &= (1 + b\,\tau)^2\,(1 - (1 + b\,\tau)(1 + 4\,b\,\tau) - (1 + b\,\tau)^2\,(1 - 2\,b^2\,\tau^2))\,, \\ p_2(b, \tau) &= b\,\tau\,(4 + 13\,b\,\tau - b^2\,\tau^2 - 31\,b^3\,\tau^3 - 22\,b^4\,\tau^4 + 8\,b^5\,\tau^5 + 12\,b^6\,\tau^6 + 3\,b^7\,\tau^7)\,, \\ p_3(b, \tau) &= (1 + b\,\tau)\,(2 + b\,\tau)\,(2 - b^2\,\tau^2)\,(1 + 2\,b\,\tau - b^2\,\tau^2 - b^3\,\tau^3)\,b^3\,\tau\,. \end{aligned}$$

As in (Rivlin, 1949) and (Nardinocchi et al., 2009), the no–traction condition $\mathbf{Tm} = \mathbf{0}$ on $\mathcal{M}_o$ turns out p_o, and completely determines the Cauchy stress. Moreover, on the inner mantle $\mathcal{M}_i$ there is a traction field $\mathbf{Tm} = -p_i\,\mathbf{m}$ different from zero with

$$p_i = c_1\,(R_o^2 - R_i^2)\left(1 + \gamma\,(R_o^2 + R_i^2)\,(1 + b\,\tau)^4\,\tau^2 - 2\gamma\,p_1\right)\tau^2 + 2\,c_1\,\gamma\,(\log\frac{b^2 + R_o^2}{b^2 + R_i^2}\,p_2 - \frac{R_o^2 - R_i^2}{(b^2 + R_i^2)(b^2 + R_o^2)}\,p_3)\,. \tag{3.15}$$

On the bases of the cylindrical structure we find a traction field $\mathbf{T}_\pm\mathbf{e}_3$ with $\mathbf{T}_\pm$ denoting the values attained by the Cauchy stress field $\mathbf{T}$ on the bases $\mathcal{D}_h$ and $\mathcal{D}_0$, respectively. It consists of an axial stress $\sigma_\pm = \mathbf{T}_\pm\mathbf{e}_3 \cdot \mathbf{e}_3$, the reaction to the kinematical constraint on the axial displacement, and a tangential stress $\mathbf{t}_\pm = (\mathbf{T}_\pm\mathbf{e}_3 - (\mathbf{T}_\pm\mathbf{e}_3 \cdot \mathbf{e}_3)\mathbf{e}_3)$, responsible for the pure torsional deformation. Then, we consider the stress resultants acting on the bases; in particular, we focus on the torque $\mathbf{M} = M\mathbf{e}_3$, and on the axial force $\mathbf{N} = N\mathbf{e}_3$

$$M = \int_{\mathcal{P}} \mathbf{x}_o \times \mathbf{t}\,d\mathbf{x}_o \cdot \mathbf{e}_3\,, \quad N = \int_{\mathcal{P}} \sigma\,d\mathbf{x}_o\,. \tag{3.16}$$

It is possible to obtain an explicit representation of the resultants in terms of the relevant material and geometrical parameters; we find

$$\begin{aligned} M &= c_1\,\pi\,(R_o^4 - R_i^4)\,\tau + M_f(R_i, R_o, b, \tau, c_1, \gamma)\,, \\ N &= -1/2\,c_1\,\pi\,(R_o^2 - R_i^2)^2\,\tau^2 + N_f(R_i, R_o, b, \tau, c_1, \gamma)\,. \end{aligned} \tag{3.17}$$

Detailed representations of M_f, N_f are given in the appendix. In $(3.17)_1$, the first summand, a linear function of τ, represents the torque competing to an isotropic and incompressible cylinder, thus corresponding to the Rivlin solution. The second summand defines the correction due to the presence of the helicoidal fibres; it is a polynomial function of τ, up to the power seven, as equation (A.29) shows.

The first summand in $(3.17)_2$, quadratic in τ, defines the axial force competing to the isotropic and incompressible pipe; it is worth noting that it vanishes in the linear approximation, that is, for small τ. The second summand defines the contribution to the axial force due to the anisotropy; such term persists in a first order approximation, as the representation formula (A.30) shows.

We find useful to represents our results highlighting the torsion angle $\hat{\varphi}$, the modulus γ, three different geometries from (Taber et al., 1996), representative of three typical ratios between outer and inner radii, fig. 2, and the

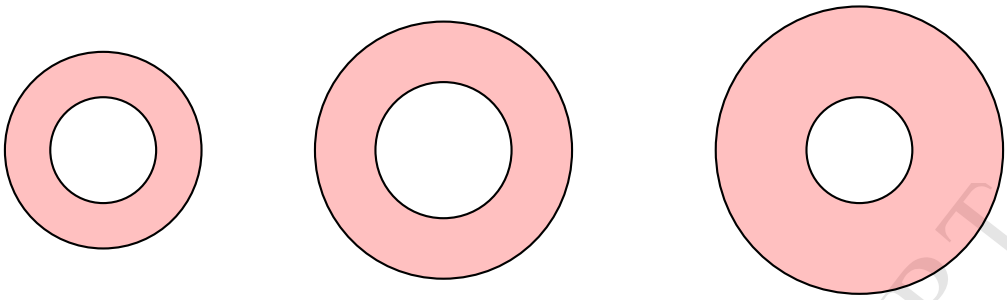

Figure 2: Geometries. From left to right: basic ($R_o/h = 0.26$ and $R_i/R_o = 0.54$), eccentric ($R_o/h = 0.34$ and $R_i/R_o = 0.53$), concentric ($R_o/h = 0.38$, and $R_i/R_o = 0.37$).

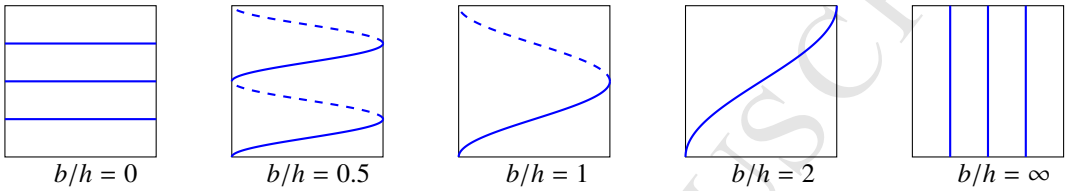

Figure 3: Different fibre windings.

dimensionless pitch b/h of the helix, fig. 3. Given a basic geometry defined by $R_o/h = 0.26$ and $R_i/R_o = 0.54$, we consider two types of excessive development of the cylindrical geometry with respect to the basic one: the eccentric geometry, characterized by an augmented wall thickness (resembling the ventricular eccentric hypertrophy), defined by $R_o/h = 0.34$ and $R_i/R_o = 0.53$, and the concentric one, showing an augmented lumen (resembling the ventricular concentric hyperthrophy), defined by $R_o/h = 0.38$, and $R_i/R_o = 0.37$.

Figures 4 and 5 show the dependence of the torque M and of the axial force N on some relevant material and geometric parameters, for the two energies we consider; dashed curve correspond to the strain energy (2.6) – I_4 reinforcement – solid curves to strain energy (2.7) – I_5 reinforcement.

Figure 4 on the left shows the behavior of the dimensionless torque $\bar{M}$, $\bar{M} = M/\pi R_o^3 c_1$ versus torsion angle $\hat{\varphi}$ for different fibre stiffness; at right, it shows $\bar{M}$ versus the winding parameter b/h, for $\hat{\varphi} = \pi/2$, $\gamma = 1$, and for three different pipe geometries. The line labeled a represents the isotropic benchmark.

As expected, the reinforcement based on I_5 (solid lines) requires larger torques with respect to that based on I_4 (dashed lines) in order to induce the same torsion angle $\hat{\varphi}$; moreover, it turns out that the torque is not a monotone function of b/h, (see figure 4, right). Figure 5 shows a remarkable difference in the axial force corresponding to the different energies we used; actually, the axial force corresponding to the I_4 reinforcement is scaled down by a factor force 10^{-3}. Moreover, there is a qualitative difference, too: when the material model associated to the invariant I_4 is used, a negative axial force is always associated to the torsion of the pipe for any value of b/h. On the contrary, when the material model I_5 is used the axial force is still negative for small b/h and positive otherwise revealing a peculiar behavior of the material model: the transition from a torsion–induced extension (corresponding to low values of b/h) to a torsion–induced shortening (corresponding to large values of b/h).

4. Pressure-induced torsional deformations

This section deals with a specific problem: torsional deformations and volume change induced on the neo-hookean fibre–reinforced pipe when it is inflated by a uniform pressure field acting on the inner mantle, and the rotation of one of its bases with respect to the axis of the pipe is constrained. For such a case, it is not possible to give an explicit solution, thus, we implement and solve the problem using a finite element analysis.

In order to tackle the incompressibility constraint, as suggested in (Ogden, 1978), we decompose the deformation gradient $\mathbf{F}$ into a spherical (dilatational), and an unimodular (distortional) part: $\mathbf{F} = J^{1/3}\bar{\mathbf{F}}$ with $J = (\det\mathbf{F})$;

accordingly, the strain measure $\mathbf{C}$ and its invariant I_1, I_4, and I_5 decompose as:

$$\mathbf{C} = J^{2/3}\,\bar{\mathbf{C}}\,, \quad I_1 = J^{2/3}\,\bar{I}_1\,, \quad I_4 = J^{2/3}\,\bar{I}_4\,, \quad I_5 = J^{4/3}\,\bar{I}_5\,, \tag{4.18}$$

with $\bar{\mathbf{C}} = \bar{\mathbf{F}}^T\bar{\mathbf{F}}$, $\bar{I}_1 = \bar{\mathbf{C}}\cdot\mathbf{I}$, $\bar{I}_4 = \bar{\mathbf{C}}\mathbf{e}_b\cdot\mathbf{e}_b$, and $\bar{I}_5 = \bar{\mathbf{C}}^2\mathbf{e}_b\cdot\mathbf{e}_b$. Moreover, we relax the incompressibility constraint, and consider the energy to be the sum of a purely isochoric contribution ψ_d and a purely volumetric one ψ_v:

$$\psi = \psi_d(\bar{\mathbf{C}}) + \psi_v(J)\,, \quad \psi_d(\bar{\mathbf{C}}) = c_1(\bar{I}_1 - 3) + c_1\gamma(\bar{I}_\alpha - 1)^2\,, \quad \psi_v(J) = \frac{1}{2}k(J-1)^2\,, \tag{4.19}$$

with $\alpha = 4, 5$ depending on the reinforcement material model. The stress $\mathbf{S} = \partial\psi/\partial\mathbf{C}$ turns out as decoupled into the distortional part $\mathbf{S}_d$ and the volumetric part $\mathbf{S}_v$. Specifically, we have

$$\mathbf{S} = \frac{\partial\psi}{\partial\mathbf{C}} = \mathbf{S}_d + \mathbf{S}_v\,. \tag{4.20}$$

The representation formula of the distortional component $\mathbf{S}_d$ depends on the reinforcement model; we have

$$\mathbf{S}_d = c_1J^{-2/3}(\mathbf{I} - \frac{1}{3}I_1\mathbf{C}^{-T}) + c_1\gamma(J^{-2/3}I_4 - 1)J^{-2/3}(\mathbf{e}_b\otimes\mathbf{e}_b - \frac{1}{3}I_4\mathbf{C}^{-T}) \tag{4.21}$$

when the standard reinforcement model (based on the invariant I_4) is accounted for and

$$\mathbf{S}_d = c_1J^{-2/3}(\mathbf{I} - \frac{1}{3}I_1\mathbf{C}^{-T}) + c_1\gamma(J^{-4/3}I_5 - 1)J^{-4/3}(\mathbf{C}\mathbf{e}_b\otimes\mathbf{e}_b + \mathbf{e}_b\otimes\mathbf{C}\mathbf{e}_b - \frac{2}{3}I_5\mathbf{C}^{-T}) \tag{4.22}$$

when the reinforcement material model based on the invariant I_5 is accounted for. As far as the volumetric component $\mathbf{S}_v$ is concerned, we have:

$$\mathbf{S}_v = \frac{1}{2}kJ(J-1)\mathbf{C}^{-T}\,. \tag{4.23}$$

The stress $\mathbf{T}$ follows as

$$\mathbf{T} = 2J^{-1}\mathbf{F}\mathbf{S}\mathbf{F}^T = \mathbf{T}_d + k(J-1)\mathbf{I} \quad , \quad \mathbf{T}_d = 2J^{-1}\mathbf{F}\mathbf{S}_d\mathbf{F}^T\,. \tag{4.24}$$

The previous equation identifies a constitutive prescription for the reactive pressure:

$$p = -k(J-1)\,, \tag{4.25}$$

which allows to write, as usual, $\mathbf{T} = \mathbf{T}_d - p\mathbf{I}$. Finally, the following (weak) elastic problem is solved through a mixed displacement-pressure formulation: find a displacement field $\mathbf{u}$ and a pressure field p such that

$$\int_{C_t} -(\mathbf{T}_d - p\mathbf{I})\cdot\nabla\tilde{\mathbf{u}} + \int_{\partial C_t}\hat{\mathbf{t}}\cdot\nabla\tilde{\mathbf{u}} = 0 \quad \text{and} \quad \int_C(\frac{p}{k} + (J-1))\tilde{p} = 0\,, \tag{4.26}$$

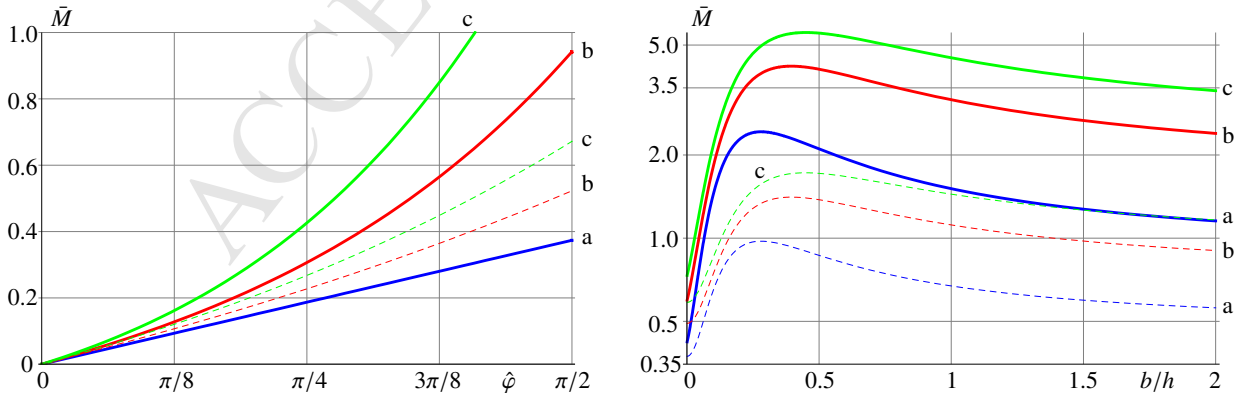

Figure 4: Torque VS $\hat{\varphi}$ for different fibre stiffness: $\gamma = 0$ (a, blue), 0.5 (b, red), 1 (c, green) (left). Torque VS b/h for different pipe geometries: ($R_o/h = 0.26, R_i/R_o = 0.54$) (a, blue), ($R_o/h = 0.34, R_i/R_o = 0.53$) (b, red), ($R_o/h = 0.38, R_i/R_o = 0.37$) (c,green), with $\gamma = 1$ and $\hat{\varphi} = \pi/2$. Solid lines refer to reinforcements I_5, dashed lines to I_4.

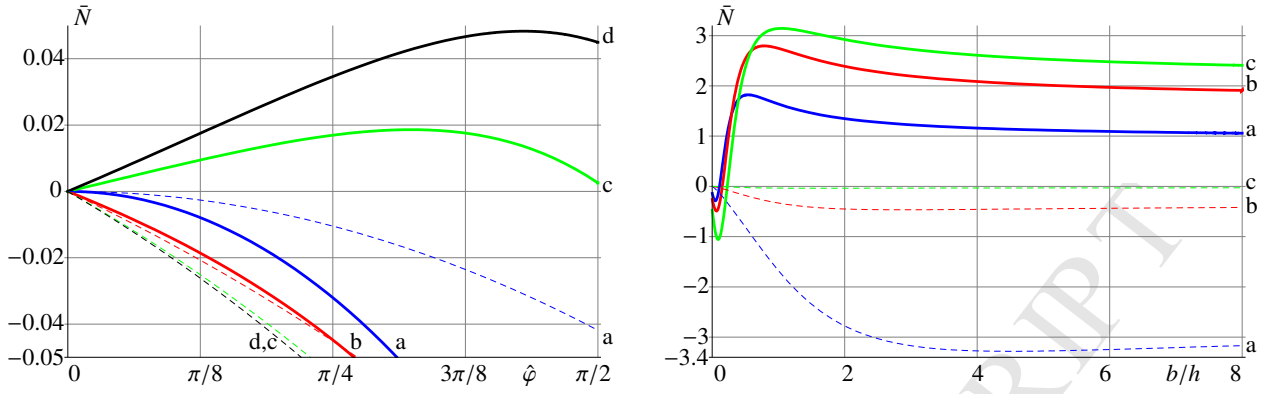

Figure 5: Axial force VS $\hat{\varphi}$ for different fibre winding: $b/h = 0$ (a, blue), 0.09 (b, red), 0.11 (c, green), 0.115 (d, black), for $\gamma = 1$ and $R_o/h = 0.26$, $R_i/R_o = 0.54$ (left). Axial force VS b/h for different pipe geometries: ($R_o/h = 0.26, R_i/R_o = 0.54$) (a, blue), ($R_o/h = 0.34, R_i/R_o = 0.53$) (b, red), ($R_o/h = 0.38, R_i/R_o = 0.37$) (c, green), with $\gamma = 1$ and $\hat{\varphi} = \pi/2$ (right). Solid lines refer to reinforcements I_5, dashed lines to I_4 (scaled by a factor 10^{-3}).

for all test field $\tilde{\mathbf{u}}$ and $\tilde{p}$. The traction $\hat{\mathbf{t}}$ is the pressure acting on the inner mantle of the pipe:

$$\hat{\mathbf{t}} = \pi \mathbf{m}\,, \quad \mathbf{m} = \frac{\mathbf{F}^* \mathbf{n}}{|\mathbf{F}^* \mathbf{n}|}\,. \tag{4.27}$$

To evaluate the torsional rotation of one base with respect to the other, we define a mean rotation angle φ_h

$$\varphi_h = \frac{\int_{\mathcal{D}_h} \varphi d\mathbf{x}_o}{\int_{\mathcal{D}_h} d\mathbf{x}_o}\,, \quad \varphi = \arctan \frac{\mathbf{u} \cdot \mathbf{n}_{,\theta}}{R + \mathbf{u} \cdot \mathbf{n}}\,. \tag{4.28}$$

With a view towards biomechanical implications, we find useful to investigate the mechanical response of the pipe under an inflating pressure field π in terms of the torsion angle of a basis with respect to the other one, and of volume change measured as the ratio between the reference volume V_0 of the cylindrical cavity and the corresponding deformed volume. Both these aspects are relevant for evaluating ventricle performance (Taber et al., 1996; Little and Braunwald, 2008).

Our first analysis concerns the effects of the two reinforcement I_4 and I_5 for a cylinder with the basic geometry ($R_o/h = 0.26$, $R_i/R_o = 0.54$), having fibres winding with constant angle $\alpha = 20°$: figure 6 shows a remarkably difference in volumetric stiffness (right), despite the small differences in torsional stiffness (left); it is worth noting the non monotone response in terms of volume change. Pressure ranges in $(0.1c_1, 1.6c_1)$, $\gamma = 0.5$; rotation is clockwise.

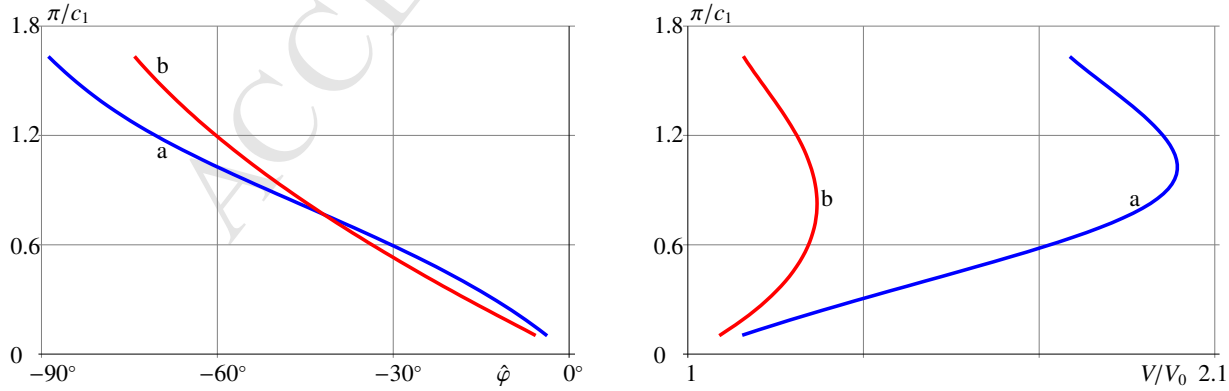

Figure 6: Comparison of I_4 (a,blue) and I_5 (b,red) reinforcement: torsion rotation (left) and change in volume (right) under inflation test; here, $\gamma = 0.5$, $\alpha = 20°$

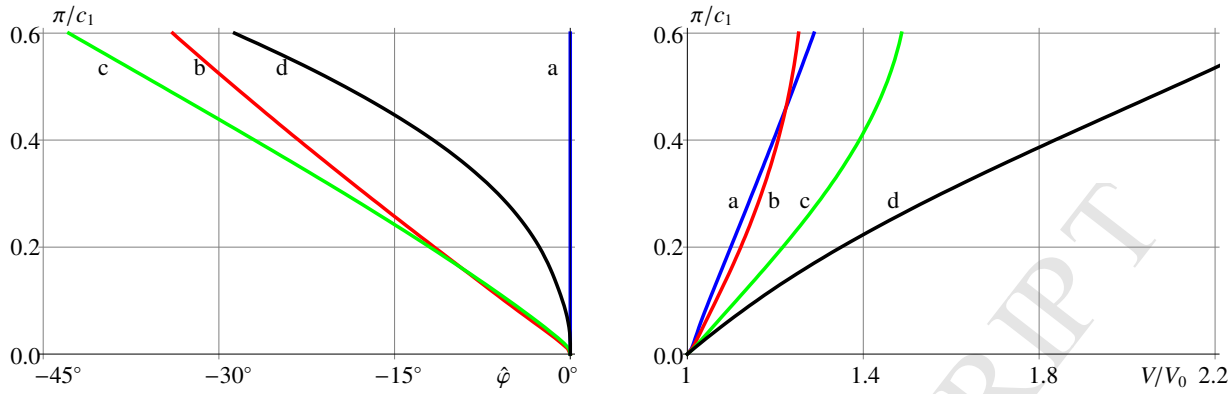

Figure 7: Pressure VS torsion angle (left) and pressure VS change in volume (right). Winding angle $\alpha = 0°$ (a, blue), 20° (b, red), 40° (c, green), 60° (d, black) (left). Reinforcement I_5 with $\gamma = 0.5$.

Next, we consider the effect that the angle of fibres winding has on I_5 reinforcement (see figure 7); the analyses concern a pipe with the basic geometry, and fibres winding with α constant across the wall thickness. As expected, pressure does not induce torsion with circumferential fibres ($\alpha = 0°$) or longitudinal fibres ($\alpha = 90°$), and it does when α takes values in between such extremes. Both torsional and volumetric stiffness depend on winding angle, and this dependence is not monotone. Moreover, volumetric stiffness, for a given α, is not a monotone function of pressure.

We conclude by analysing two other cases: a basic geometry with a linear variation of the angle α across the wall thickness, and, for a given fibre winding, the three different pipe geometries.

Figure 8 shows the response under inflating pressure for a pipe with basic geometry, having fibres winding linearly varying from −60° at the outer mantle, to 60° at the inner mantle. Within the range of γ we consider, both torsional and volumetric stiffness are not monotone. Figure 9 shows the results of inflation test for three different geometries, see Fig. 2; here, $\alpha = 20°$ and $\gamma = 0.5$. With respect to the basic geometry, the eccentric one is characterized by a larger lumen and an augmented wall thickness so as to keep the ratio midwall-radius/wall-thickness almost normal, thus resembling the ventricular eccentric hypertrophy, that in heart is related to volume overloading. The concentric geometry has a smaller lumen and an exaggerate wall thickness; it is intended to resemble the ventricular concentric hypertrophy, that in heart is related to pressure overloading. It is worth noting that, for a given fibre winding and stiffness γ, geometry has a large effect on volumetric stiffness (right).

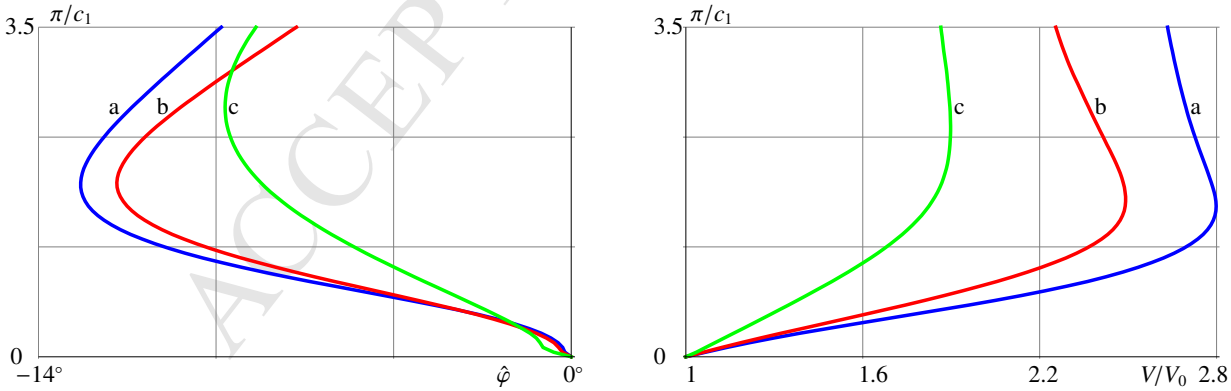

Figure 8: Pressure VS torsion (left) and pressure VS change in volume (right) with fibres winding linearly varying from −60° at the outer mantle, to 60° at the inner mantle. Stiffness γ is 0.05 (a, blue), 0.1 (b, red), 0.5 (c, green).

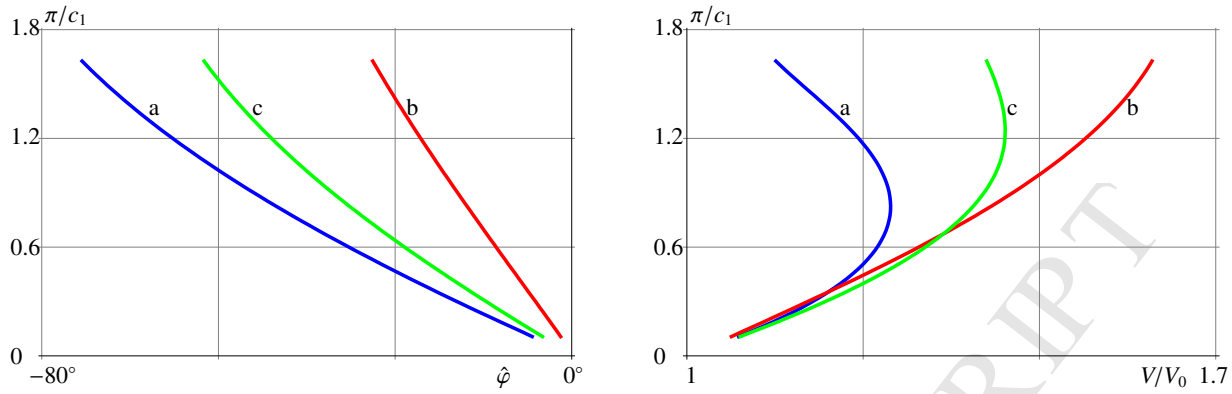

Figure 9: Inflation test for three different geometries: pressure VS torsion (left) and pressure VS change of volume (right); basic (a, blue), concentric (b, red), eccentric (c, green), $\alpha = 20°$, $\gamma = 0.5$.

Appendix.

The explicit representation form of the torque and the axial force in terms of the relevant material and geometrical parameters is here given. Both the torque and the axial force are represented as polynomial function of τ:

$$\begin{aligned}
M/c_1 = {} & (\pi(R_o^4 - R_i^4) + \pi\gamma 16b^2(f_2(2b^4 + f_5 + b^2 f_4) + 2b^2 f_1))\tau + \\
& + \pi\gamma(f_2(36b^7 + 24b^3 f_5 + f_4(18b^5 + 6bf_5) + 6b^3 f_6) + 36b^5 f_1)\tau^2 + \\
& + \pi\gamma(f_2(-88b^8 - \tfrac{70}{3}b^4 f_5 + f_4(-44b^6 + \tfrac{62}{3}b^2 f_5) + \tfrac{62}{3}b^4 f_6 + \tfrac{2}{3}b^2 f_4 f_6 + \tfrac{2}{3}f_5 f_7) - 88b^6 f_1)\tau^3 + \\
& + \pi\gamma(f_2(-110b^9 + \tfrac{55}{3}b^5 f_3^2 + f_4(-55b^7 + \tfrac{55}{3}b^3 f_5) + \tfrac{10}{3}b^3 f_4 f_6 + \tfrac{10}{3}bf_5 f_7) - 110b^7 f_1)\tau^4 + \\
& + \pi\gamma(3b^2 f_3(6b^4 - 3b^2 f_4 + 2f_7) + 18b^8 f_1)\tau^5 + \\
& + \pi\gamma(f_2(56b^{11} + f_3^2(-\tfrac{28}{3}b^7 + \tfrac{14}{3}b^5 f_4) + 28b^9 f_4 + \tfrac{14}{3}b^3 f_5 f_7) + 56b^9 f_1)\tau^6 + \\
& + \pi\gamma(f_2(16b^{12} + f_3^2(-\tfrac{8}{3}b^8 + \tfrac{4}{3}b^6 f_4) + 8b^{10} f_4 + \tfrac{4}{3}b^4 f_5 f_7) + 16b^{10} f_1)\tau^7
\end{aligned} \tag{A.29}$$

and

$$\begin{aligned}
N/c_1 = {} & -\pi\gamma(8bf_3 + f_8 8b^3 + 16b^5 f_2 + (24b^3 + 8bf_{10})f_1)\tau - \\
& - \pi(\tfrac{1}{2}f_3^2 + \gamma(26b^2 f_3 + f_8 28b^4 - f_2 4b^2(7b^4 + 5f_5 + 5b^2 f_4) + f_9(b^4 + f_5 + b^2 f_4) + 26b^2 f_{10} f_1))\tau^2 - \\
& - \pi\gamma(-f_2 12b(5b^6 + 3b^2 f_5 + \tfrac{5}{2}b^4 f_4 + \tfrac{1}{6}f_5 f_4) - 2b^3 f_3 + f_8 16b^5 + \\
& \quad + f_9 9b(b^4 + f_5 + b^2 f_4 - \tfrac{2}{9}b^2 f_3) - (44b^5 + 2b^3 f_{10})f_1)\tau^3 - \\
& - \pi\gamma(+f_9(18b^6 + 18b^2 f_5 + \tfrac{1}{3}f_5 f_{11} + \tfrac{73}{3}b^4 f_4 + \tfrac{1}{3}b^2 R_i^2 f_4 + \tfrac{2}{3}b^2 R_o^2 f_4) - \\
& \quad - 62b^4 f_3 - f_8 26b^6 + f_2(4b^8 - \tfrac{13}{3}b^4 f_5 - \tfrac{35}{3}b^4 R_o^4 + 2b^6 f_4 - 6b^2 f_5 f_4) - (22b^6 + 62b^4 f_{10})f_1)\tau^4 - \\
& - \pi\gamma(+f_9(9b^7 + 9b^3 f_5 + \tfrac{2}{3}b^5(11R_i^2 - 5R_o^2) + \tfrac{4}{3}bf_5 f_{11} + 9b^5 f_4 + \tfrac{2}{3}b^3 f_4(2R_i^2 + 13R_o^2)) - \\
& \quad - 44b^5 f_3 - f_8 26b^7 + f_2(36b^9 + 18b^7 f_4 - 6b^3 R_o^4 f_4) + (10b^7 - 44b^5 f_{10})f_1)\tau^5 - \\
& - \pi\gamma(-f_9(7b^8 + 7b^4 f_5 + 7b^6 f_4 - 4b^4 R_o^2 f_4 - 2b^6(R_o^2 + 2R_i^2) - 2b^2 f_5 f_{11}) + 16b^6 f_3 + f_8 2b^8 + \\
& \quad + f_2(12b^{10} + 6b^8 f_4 - 2b^4 R_i^4 f_4) + (14b^8 + 16b^6 f_{10})f_1)\tau^6 - \\
& - \pi\gamma(-f_9(8b^9 + 8b^5 f_5 + 8b^7 f_4) + 24b^7 f_3 + f_8 8b^9 + \tfrac{4}{3}b^3 f_3^2 f_{11} + (8b^9 + 24b^7 f_{10})f_1)\tau^7 - \\
& - \pi\gamma(-f_9(2b^{10} + 2b^6 f_5 + 2b^8 f_4) + 6b^8 f_3 + f_8 2b^{10} + \tfrac{1}{3}b^4 f_3^2 f_{11} + (2b^{10} + 6b^8 f_{10})f_1)\tau^8 .
\end{aligned} \tag{A.30}$$

In (A.29) and (A.30), the functions f_i, $(i = 1, 9)$ are defined as

$$f_1(Ro, Ri, b) = \log \frac{b^2 + R_i^2}{b^2 + R_o^2}\,, \quad f_2(Ro, Ri, b) = \frac{R_o^2 - R_i^2}{(b^2 + R_i^2)(b^2 + R_o^2)}\,, \quad f_3(Ro, Ri) = R_o^2 - R_i^2\,, \tag{A.31}$$

$$f_4(Ro, Ri) = R_o^2 + R_i^2\,, \quad f_5(Ro, Ri) = R_i^2 R_o^2\,, \tag{A.32}$$

$$f_6(Ro, Ri) = R_o^4 + R_i^4\,, \quad f_7(Ro, Ri) = R_o^4 + R_o^2 R_i^2 + R_i^4\,, \tag{A.33}$$

$$f_8(Ro, Ri, b) = \frac{R_o^2 - R_i^2}{b^2 + R_o^2}\,, \quad f_9(Ro, Ri, b) = \frac{(R_o^2 - R_i^2)^2}{(b^2 + R_i^2)(b^2 + R_o^2)}\,, \tag{A.34}$$

$$f_{10}(Ri, b) = b^2 + R_i^2\,, \quad f_{11}(Ro, Ri) = R_i^2 + 2R_o^2\,. \tag{A.35}$$

References

DiCarlo, A., Nardinocchi, P., Svaton, T., Teresi, L., 2009. Passive and active deformation process in cardiac tissue. Proceedings of the Int. Conf. on Computational Methods for Coupled Problems in Science and Engineering (COUPLED PROBLEMS 2009), Eds. B. Schreer, E. Onate and M. Papadrakakis, CIMNE, Barcelona, 2009.

Gasser, T.C., Ogden, R.W., Holzapfel, G.A., (2006). Hyperelastic modelling of arterial layers with distributed collagen fibre orientation. J.R.Soc. Interface, 3, 15–35.

Holzapfel, G.A., Gasser, T.C., Ogden, R.W., 2000. A New Constitutive Framework for Arterial Wall Mechanics and a Comparative Study of Material Models. Journal of Elasticity, 61, 1-48.

Holzapfel, G.A., Gasser, T.C., Ogden, R.W., 2004. Comparison of a Multi-Layer Structural Model for Arterial Walls With a Fung-Type Model, and Issues of Material Stability. Journal of Biomechanical Engineering, 126, 264–275.

Little W.C., Braunwald, E., 2008. Assessment of cardiac function. In: Braunwald's Heart Disease. A Textbook of Cardiovascular Medicine. Eighth Edition. Eds: Libby, P., Bonow, R.O., Mann, D.L., Zipes, D.P., 421–445.

Merodio, J., Ogden, R.W., 2005. Mechanical response of fibre-reinforced incompressible non-linearly elastic solids. International Journal of Non-Linear Mechanics, 40, 213–227.

Nagel, E., Stuber, M., Burkhard, B., Fischer, S.E, Scheidegger, M.B, Boesiger, P., Hess, O.M.. (2000) European Heart Journal, 21(7), 582–589.

Nardinocchi, P., Svaton, T., Teresi, L., (2009). Mechanical response of helically wound fibre-reinforced incompressible non-linearly elastic pipes. In press on Lecture Notes in Applied and Computational Mechanics, Springer.

Ogden, R.W., 1978. Nearly isochoric elastic deformations: Application to rubberlike solids. J. Mech. Phys. Solids 26 (1978) 3757. 42.

Rivlin, R.S., 1949. A note on the torsion of an incompressible highly-elastic cylinder. Proc. Cambridge Philos. Soc. **45**, 485–487.

Taber, L.A., Yang, M., Podszus, W.W., (1996). Mechanics of Ventricular Torsion. J. Biomechanics, 29(6), 745–752.